AUTOMATIC GENERATION OF DIGITAL TERRAIN MODELS FROM CARTOSAT-1 STEREO IMAGES

Hossein Arefi [a], Pablo d'Angelo [a], Helmut Mayer [b] and Peter Reinartz [a]

[a] German Aerospace Center (DLR),
D-82234 Wessling, Germany
(hossein.arefi, pablo.angelo, peter.reinartz)@dlr.de

[b] Institute for Applied Computer Science
Bundeswehr University Munich, D-85577 Neubiberg, Germany
helmut.mayer@unibw.de

Commission I, WG 4

KEY WORDS: Digital Surface Models (DSM), Digital Terrain Models (DTM), CARTOSAT-1, image matching, gray-scale reconstruction, morphological processing, segmentation, non-ground regions

ABSTRACT:

This paper proposes a novel algorithm for automatic Digital Terrain Model (DTM) generation from high resolution CARTOSAT-1 satellite images generating accurate and reliable results. It consists of two major steps: Generation of Digital Surface Models (DSM) from CARTOSAT-1 stereo scenes and hierarchical image filtering for DTM generation.
High resolution stereo satellite imagery is well suited for the creation of DSM. A system for automated and operational DSM and orthoimage generation based on CARTOSAT-1 imagery is presented, with emphasis on fully automated georeferencing. It processes level-1 stereo scenes using the rational polynomial coefficients (RPC) universal sensor model. A novel, automatic georeferencing method is used to derive a high quality RPC correction from lower resolution reference dataset, such as Landsat ETM+ Geocover and SRTM C Band DSM. Digital surface models (DSM) are derived from dense stereo matching and forward intersection and subsequent interpolation into a regular grid.
In the second step which is dedicated to DSM filtering, the DSM pixels are classified into ground and non-ground using the algorithm motivated from the gray-scale image reconstruction to suppress unwanted elevated pixels. In this method, non-ground regions, i.e., 3D objects as well as outliers (very low or very high elevated regions) are hierarchically separated from the ground regions.
The generated DTM is qualitatively and quantitatively evaluated. Profiles in the image as well as a comparison of the derived DTM to the original data and ground truth data are presented. The ground truth data consist of a high quality DTM produced from aerial images which is generated by the Institut Cartografic de Catalunya (ICC) in Barcelona, Spain. The evaluation result indicates that almost all non-ground objects regardless of their size are eliminated and the iterative approach gives good results in hilly as well as smooth residential areas.

1 INTRODUCTION

High resolution CARTOSAT-1 stereo satellite imagery is well suited for the generation of DSM. A fully automated DSM generation system processes photometrically corrected level-1 stereo scenes. Robust stereo matching on epipolar images and outlier removal are employed to estimate high quality stereo tie points. An affine correction of the rational polynomial coefficients (RPC) universal sensor model delivered with the CARTOSAT-1 images is performed using the Landsat ETM+ and Shuttle Radar Topography Mission (SRTM) databases as reference. It is worthwhile to note that SRTM has a much higher lateral accuracy than the Landsat ETM+ mosaic, which can be used to improve the accuracy of both DSM and orthorectified images. Thus, affine RPC correction parameters are estimated by aligning a preliminary DSM to the SRTM DSM, resulting in significantly improved Geo-location of both DSM and orthoimages. After forward intersection, additional outlier removal is done based on large deviations from the SRTM data as well as local statistics of the point cloud. The result is a DSM on a 10 m grid. Remaining holes in the DSM are filled with SRTM data using the delta surface fill algorithm (Grohman et al., 2006). Check against independent ground truth indicates a lateral accuracy of 3-4 meters and a height accuracy of 4-5 meters. Independently processed scenes align at sub-pixel level and the result is therefore well suited for mosaicing. More details about the proposed stereo matching algorithm in this paper to create DSM can be found in (d'Angelo et al., 2009).
In this paper the most focus is on the second step which is about proposed DTM generation algorithm. The goal of the DTM generation step is to suppress unwanted 3D regions, e.g., buildings, trees, and outliers, using a hierarchical filtering method. The motivation of this work comes from the algorithm used for gray scale image reconstruction proposed by Vincent (1993).
The paper is organized as follows. We first review the related work in Section 2. In Section 3, we give a detailed description of our proposed DTM generation algorithm. Experimental results are presented in Section 4. Finally, we conclude our paper and discuss future work in Section 5.

2 RELATED WORK

To generate a high quality DTM from DSM data, 3D non-ground points as well as outliers have to be separated from the ground points. Various techniques and filtering methods have been proposed to generate DTM from DSM data. The DSM data can be either directly acquired such as airborne LIDAR or generated by stereo matching techniques.
Kilian et al. (1996) presented ideas on how to generate a DTM from LIDAR data recorded in wooded areas based on gray-scale morphological opening. The lowest points within a window of

a given size are first detected by an opening. Then the points in this window, that fall within a band above the lowest elevation are considered as ground points and a weighted surface interpolation using these points is applied to compute the DTM. A conclusion of this work was that the size of the Structuring Element (SE) used for opening is a critical parameter for which there is no single optimal value. Therefore, the use of multiple openings with different sizes for the SE was suggested. Kraus and Pfeifer (1998) introduced another algorithm for DTM generation in wooded areas based on linear prediction. They also start with an approximation of the ground surface. The distances from the ground surface to the measured points are used to define weights which are employed in computing the DTM based on linear prediction. If the height residual within the surface interpolation is above a certain threshold, the corresponding point is classified as " non-ground" and eliminated from the surface interpolation.
Axelsson (1999) described a method for DTM generation based on the progressive densification of a triangular irregular network (TIN). The idea is to fit a surface from below to the point cloud. In every iteration the surface is allowed to fluctuate within a certain range and points from the point cloud are added to the TIN. It is iterated until no further low ground points can be added. The approach has been built in the TerraScan software package (Terrasolid, 2007).
Vosselman (2000) proposed a slope based filtering method for separating non-ground points from ground points. A point is classified as a terrain point if there is no other point in its vicinity to which the height difference is larger than an allowed maximum difference. The method assumes that the terrain slopes do not exceed a certain threshold and the features having slopes above the thresholds are non-ground objects. The assumption limits the approach to terrain with gentle slopes. A modified slope based filtering was proposed based on varying the threshold value according to the terrain slope (Sithole, 2001).
Wack and Wimmer (2002) proposed a hierarchical grid-based approach for the generation of DTMs from airborne laser data. They start with a coarse grid of $9m$ width and define the raster height by selecting the height within the raster element for which 99% of all points are higher. The Laplacian of Gaussian (LoG) operator in combination with a weight function is used to detect and remove points that are not considered to be ground points. A progressive morphological filtering method was developed by Zhang et al. (2003) with the focus to exclude the non-ground measurements from LIDAR datasets. The algorithm applies morphological opening and gradually increases the size of the SE. The resulting elevation differences are used to classify ground and non-ground points by exerting a threshold which depends on the SE size. An unsupervised statistical skewness balancing segmentation algorithm is considered by Bartels and Wei (2006) to detach non-ground regions from the ground regions. It is based on the assumption that the naturally measured samples lead to a normal distribution and non-ground objects disturb this distribution. A recursive point removal based on the skewness is used until a normal distribution is achieved.

2.1 Morphological Reconstruction

In this paper the DTM generation algorithm is in major part motivated from the "Fast Hybrid Gray scale Reconstruction" algorithm described on Vincent (1993). The goal of the morphological reconstruction procedure is to suppress unwanted regions of high intensity signal while preserving signal intensity in the regions of interest, which are seeded with "markers" in order to initialize the algorithm (Robinson and Whelan, 2004).
"Morphological Reconstruction" is a very useful operator provided by mathematical morphology which is relatively well-known in the binary image processing. The operator extracts the connected components of an image, which are "marked" by another image. However, the algorithm operates based on a geodesic distance operator (Lantuejoul and Maisonneuve, 1984) and is extended for gray scale images as well which has been so far applied for many image analysis applications such as segmentation and filtering processes. Moreover, in photogrammetry the morphological reconstruction operation has assisted segmentation and filtering of DSM and LIDAR images (Arefi and Hahn, 2005; Arefi et al., 2007).
Gray scale reconstruction based on geodesic dilation employs

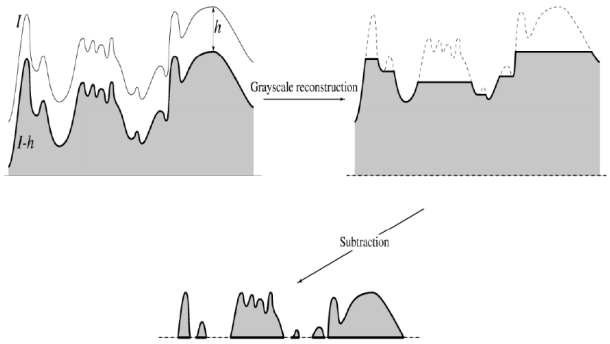

Figure 1: Reconstruction by geodesic dilation of a mask I from a marker J. The marker is produced by subtraction of a constant offset h from the mask. The result of gray scale reconstruction using geodesic dilation is shown in the top right part. The subtraction of the reconstructed signal from the mask signal leads to the result given on the bottom (Vincent, 1993)

two input images as "marker" and "mask" images. The marker image is dilated by an elementary isotropic structuring element and the resulting image is forced to remain below the mask image. This means, the mask image acts as a limit for the dilated marker image. This technique is the standard way to perform image reconstruction by geodesic dilation. Here, combined basic dilation and point-wise minimum operations are iterated until stability. Figure 1 visualizes the result of image reconstruction by dilation. Morphology dilation of marker J and point wise minimum between dilated image and mask I is employed iteratively until stability. In this example, the marker image J is produced by subtraction of an offset h from the mask I therefore, after gray scale reconstruction the upper part of the foreground regions are suppressed (cf. Figure 1, top right). The maximum height of the suppressed parts is equal to offset value h. After subtraction of reconstructed image from the original mask image, an image is produced which has been applied for removing uneven background effects in image processing. If the gray scale reconstruction operates ideally the result following subtraction is more comparable to what is called normalize DSM (nDSM) in photogrammetric image processing application.
Depending on the size of the image the number of iteration increases and therefore, the procedure becomes very time consuming. Vincent (1993) proposed a fast and efficient algorithm for gray scale image reconstruction by dilation which is titled as "Fast Hybrid Reconstruction Algorithm". The algorithm operates as follows:

- I : mask image
- J : marker image, defined on domain D_I; (mask must always be greater than or equal to the marker image)
- Scan D_I in raster order:
  - Let p be the current pixel;

- $J(p) = (max\{J(q), q \in N_G^+(p) \cup \{p\}\}) \wedge I(p)$

- Scan D_I in anti-raster order:
  - Let p be the current pixel;
  - $J(p) = (max\{J(q), q \in N_G^-(p) \cup \{p\}\}) \wedge I(p)$
  - If there exist $q \in N_G^-(p)$ such that $J(q) < J(p)$ and $J(q) < I(q)$ then *fifo_add(q)*

- Propagation step: While (!fifo_empty)
  - p = fifo_first()
  - For every pixel $q \in N_G(p)$:
    - If $J(q) < J(p)$ and $I(q) \neq J(q)$ then $J(q) = \min\{J(p), I(q)\}$ *fifo_add(q)*

where $N_G(p)$ denotes the neighborhood of p on a grid G, with N^+ and N^- denoting the neighboring pixels of pixel p which are involved for raster and anti-raster scan filtering. $\wedge$ is the point wise minimum operator (Vincent, 1993) (cf. Figure 2).

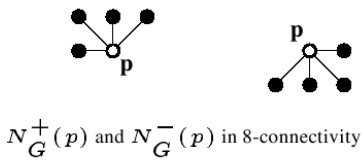

Figure 2: Neighboring pixels for filtering of point p in raster (left to right) and anti-raster (right to left) order scanning in hybrid geodesic dilation algorithm. In raster order scanning the neighboring points highlighted in $N_G^+(p)$ are points before p and $N_G^-(p)$ are the points after p where, in anti-raster scanning it is vise versa.

3 PROPOSED DTM GENERATION ALGORITHM

In DTM generation, non-ground regions are filtered from the original range image which is more similar to the task in gray scale image reconstruction that the "high density" pixels are suppressed. Therefore, the method employed in morphological reconstruction can be utilized in DTM generation as preliminary framework. The word " high density" should be first re-interpreted based on 3D objects in the surface which are interested to be filtered. Here, the non-ground regions contain all the 3D elevated artificial objects such as buildings, bridges, vehicles as well as natural objects such as trees, vegetation and bushes. In this definition high elevated grounds such as hills are excluded therefore, having high density, or here high range value, is not sufficient to categorize the object as non-ground region.

In order to separate non-ground and ground regions using geodesic dilation method, the algorithm needs to be re-formulated. As appeared in Figure 1 the height of the object to be filtered is very much depending on the offset value h for creating marker image. Selection of a small offset value filters low height objects or just the upper part of the high objects, e.g., roof top in buildings, whereas determination of a big one might filter whole object, e.g., building with part of the hill below it if it is located on a hilly terrain (cf. Figure 3). The suitable offset value to filter the building that is displayed in Figure 3 is a value between $h1$ and $h2$ (cf. Figure 3, lower row). Hence, selecting of an appropriate offset is critical.

In an earlier work, a sequence of the offset values has been chosen for image reconstruction to extract all the 3D objects appropriately (Arefi et al., 2007). To exclude unwanted objects such as hills the regions are evaluated by calculating the height discontinuity on the region boundary. The hills contain very small height discontinuity on their boundaries comparing to other 3D objects such as buildings and trees. In order to evaluate the regions, the image provided after subtraction of reconstructed image from original image, i.e., initial nDSM (cf. Figure 1, below), needs to be segmented by thresholding. For all regions produced after connected components labeling the boundary pixels are extracted and corresponding average height discontinuity for each region is computed. Only the regions having average height discontinuity on their boundary higher than a predefined value, e.g., 2m, are classified as non-ground. This procedure is continued for all other offset h values and at the end the non-ground regions are integrated in a single binary image. All the corresponding pixels in binary image are eliminated from the original image to remain only ground pixels. Next, DTM in generated by filling the gaps using interpolation method.

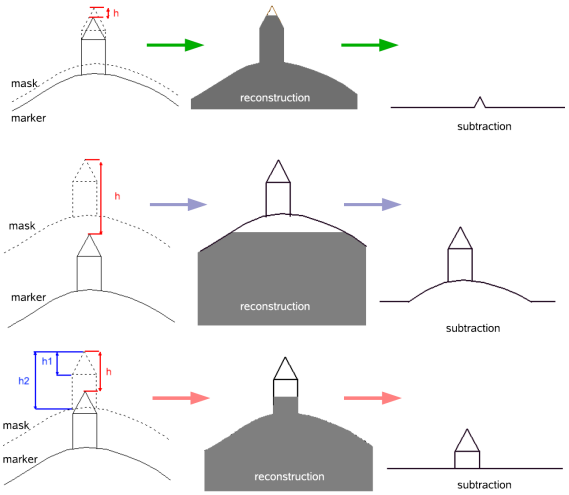

Figure 3: Selecting offset value to produce marker image

The above-mentioned procedure is iterated several times according to the number of offset values for creating marker images. The number and the values of offsets h are computed based on the maximum height discontinuity available in the scene. For that an image feature is created by computing the subtraction of minimum and maximum heights in every 3×3 window which highlights the local height variation in the image. The quality of the DTM generated using this method is quite acceptable (cf. (Arefi and Hahn, 2005; Arefi et al., 2007)) however it is a bit slow particularly in the regions like hilly residential areas where the height variations are so large.

In this paper, a new algorithm for DTM generation is proposed based on modifying the above-mentioned method and re-formulating the image reconstruction definition. Here, only a single marker image J is used which is provided from original DSM image, i.e., mask I, as follows:

$$J(i,j) = \begin{cases} I(i,j) & \text{if point } p(i,j) \text{ lies on the border of } I \\ min(I) & \text{otherwise} \end{cases} \quad (1)$$

Accordingly, the bordering pixels of the marker image remain intact comparing to the mask and the rest of the pixels get the minimum gray value of the mask. In this method the filtering of the marker image begins from the four corners of the marker im-

age sequentially. We denote by $N_G(p)$ the set of the neighbors of pixel p for grid G in 8-connectivity. In the proposed algorithm, as mentioned, we consider to filter the image from four corners to the end of the image, i.e, from upper-left (UL) corner to lower-right (LR), from LR to UL, from upper-right (UR) to lower-left (LL) and from LL to UR. To evaluate each pixel p the gray values of the pixels in the raster order and anti-raster order are considered. E.g., in process from UL to LR the three pixels of $N_G^{++}(p)$ as raster order pixels and $N_G^{--}(p)$ as anti-raster order are taken into account, where, $N_G^{++}(p)$ is the set of the neighbors of p which are reached before p during a UL to LR raster scan of the image and $N_G^{--}(p)$ consists of the neighbors of p which are reached after p. These notions are recalled on Figure 4. All the

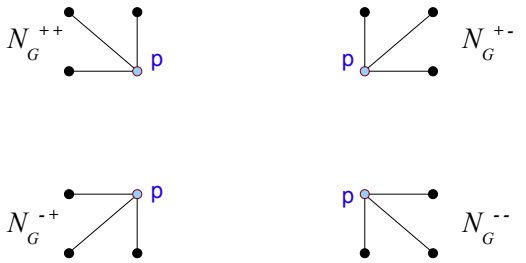

Figure 4: Neighboring pixels for filtering of point p in raster and anti-raster order scanning in hybrid geodesic dilation algorithm. In raster scan, e.g., from UL to LR the points in $N_G^{++}(p)$ are before and points in $N_G^{--}(p)$ are after point p. The same procedure takes place for other scanning orders.

pixels except the bordering ones are evaluated. Process begins by producing marker J and mask I images. In the first iteration, $I = DSM$ and J creates according to the Eq. (1). Figure 5(a) represents a section view of mask (black) and marker (dark gray) images. As shown, marker image contains pixel values with minimum gray value of mask except in the border where the gray values are equal to the mask. The filtering begins from upper-left corner and according to the raster order N_G^{++}. It employs different behaviors depending on the surface shape in local region around the point to be filtered. To categorize the ground surface shapes the following parameters should be computed in advance:

– *Let p be the current pixel;*

$$max_{(J)}^{+} = max\{J(q), q \in N_G^{++}(p) \cup \{p\}\}$$
$$max_{(I)}^{-} = max\{I(q), q \in N_G^{--}(p) \cup \{p\}\}$$
$$dH = max_{(I)}^{-} - max_{(J)}^{+}$$

The filtering procedure opreates diffrently for the following three surface shapes:

1. Terrain height monotonically decreases: The height variation between the gray values before the point p in marker J and after the point in the mask I is small, i.e., less than predefined threshold, and the points after p are lower. In this case, first the maximum values of the three neighboring pixels before p (cf. Figure 4) is computed and then it is forced to remain below or equal to the mask, i.e., a point wise minimum is employed. Figure 5(b) shows that the process begins from the second pixel $p1$ and it takes first the maximum value of the gray values in the left side (in section view only one pixel is visible). After the point wise minimum the pixel is forced down to remain equal to the mask (cf. Figure 5(c)). Since the terrain heights monotonically decrease after this pixel and before the building, the process continues and the marker image takes the mask values for these pixels. Practically the process in this step can be summarized as:

$$\textit{if} \quad (\, dH < thresh \quad \textit{and} \quad dH < 0\,)$$
$$\textit{then} \quad J(p) = max_{(J)}^{+} \wedge I(p)$$

where $\wedge$ denotes point wise minimum.

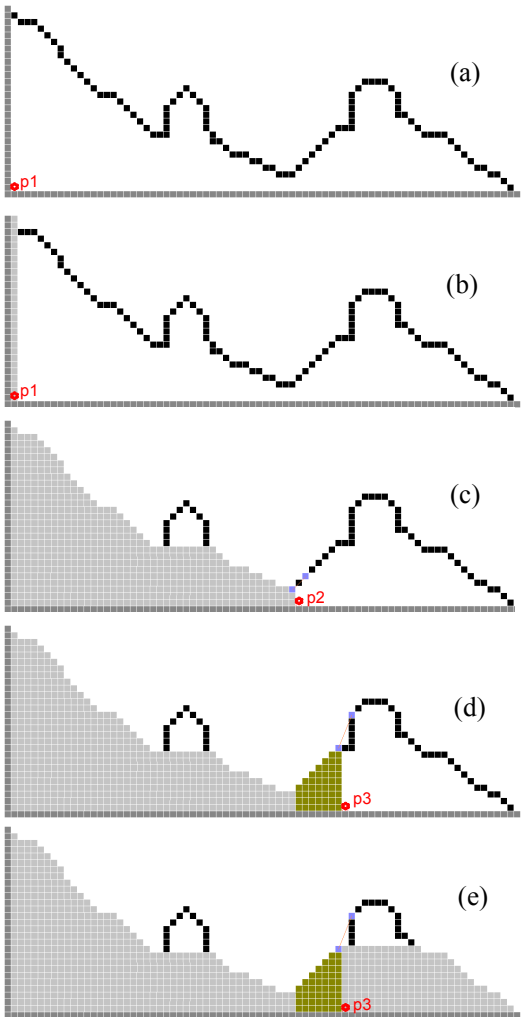

Figure 5: Filtering of non-ground regions based on proposed method

2. High elevated objects: The height variation between the gray values before the point in the marker J and after the point in the mask I is high, i.e., bigger than predefined threshold,i.e., facing with a high jump. Same process as former step is employed here and the point wise minimum between the maximum values in the neighboring (cf. Figure 4) of marker and mask. As shown in Figure 5(c), in this case, the marker image excludes the building pixels and continues below that. After the building the terrain heights again decrease monotonically for some pixels therefore, the filtering process continues according to the step 1. Practically the process in this step can be summarized as:

$$\textit{if} \quad (\, dH > thresh\,) \quad \textit{then} \quad J(p) = max_{(J)}^{+} \wedge I(p)$$

3. Terrain height monotonically increases: The height varia-

tion between the gray values before the point p in marker J and after the point p in the mask I is small, i.e., less than predefined threshold, and the points after p are higher. In this case the marker image takes the mask value. The process in this step is depicted in Figure 5(d) with jade-green color and it is practically summarized as:

$$if \quad (0 < dH < thresh) \qquad then \quad J(p) = I(p)$$

The filtering procedure continues to the end of image according to the first scanning order. Figure 5(e) shows the final result of the filtering from left to right. For an ideal filtering to remove all above ground regions the process needs to iterate and use other scanning directions for filtering. It is very important to mention that after each iteration the filtered marker image will be selected as mask for the next iteration but the marker always take the initial one, i.e., according to Eq. (1).
So far the filtering approach for separating above groung regions from ground regions have been finished. If we assume that the DSM often contains many below the ground outliers therefore, the process should include an outliers removal algorithm. The procedure to eliminate below the ground outliers are almost same as above ground objects, unless it applies on the image complement of DSM. For that first the maximum gray value of DSM is computed and then all the gray values are subtracted from this value to produce complemented image. Now the process repeated using new mask image, i.e., complemented DSM (cDSM). Since in DTM the objects such as underground entrance or underground stairs are included therefore, the threshold value $thresh$ should tune in case that only the regions that are much below their surrounding pixels, e.g., $10m$, be eliminated.

4 EXPERIMENTAL RESULTS

To evaluate the proposed method for DTM generation a hilly residential area which covers also parts of the city of Barcelona in Spain is used as an example. A DSM is generated using stereo matching algorithm in 10m grid resolution. It contains many gaps produced from mismatched regions. The gaps are filled with SRTM data and using the delta surface fill algorithm (Grohman et al., 2006). Figures 6(a) and 6(b) show the created DSM before and after gap filling. The regions that are highlighted with very dark color in Figure 6(a) represent the mismatched areas which are mostly water body regions (mainly ocean) and flat cultivated fields.
For DTM generation a threshold ($thresh$) value of $2m$ has been selected for evaluating above ground objects. The pixel which is higher than $2m$ with respect to previously classified pixel as ground, will be suppressed using point wise minimum operation and classified as non-ground object. As mentioned, the marker image has the same pixel values on its borders with the mask image. The processing of the first pixels after bordering ones checks if the candidate pixel is higher than the previous pixel, i.e., in border, or not. If not it assumes that the pixel is ground and should not be filtered. Since the bordering pixels are not always located on the ground surface therefore, the 3D regions which are partly connected to the image boundary will not be filtered. The algorithm tries to suppress these objects when the procedure begins from other corners of image but the effects is not completely eliminated. therefore the quality of the filtering algorithm is lower if there exists 3D objects connected to the image boundary.
Figure 6(c) represents the final DTM created based on the proposed algorithm in this paper. Comparing the produced DTM (cf. Figure 6(c)) and ICC reference DTM (cf. Figure 6(d)) shows that there are some clear differences between these two images. The elevated roads that are clearly higher than the neighboring

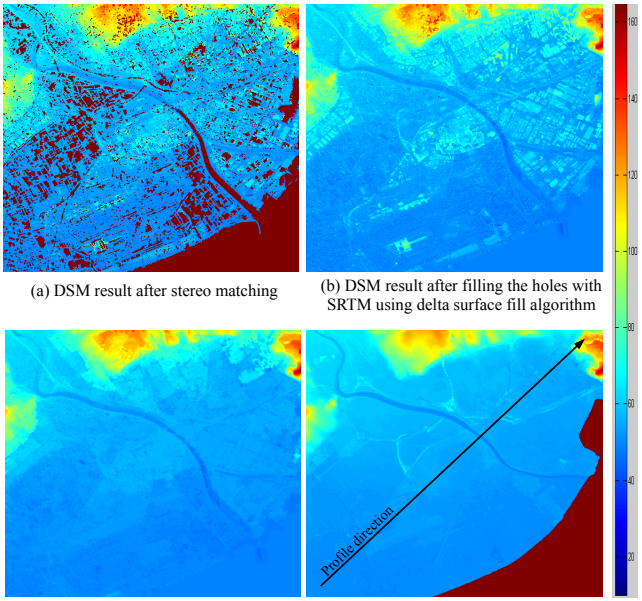

(a) DSM result after stereo matching
(b) DSM result after filling the holes with SRTM using delta surface fill algorithm
(c) DTM generated using proposed algorithm
(d) ICC reference DTM

Figure 6: Representing input and output surface models as well as the reference DTM for quality assessment

pixels are not eliminated from the reference DTM. They are minimum $5m$ higher than the neighboring terrain surfaces. The other problem is that, there exists some objects such as rivers and roads that are available in one dataset and not in the other one. This is most probably due to difference in the acquiring time between CARTOSAT-1 and the aerial photos to generate corresponding surface models.
In addition to visually evaluating the results, a profile has been provided along the image and is plotted in Figure 7. The location of the profile is shown in Figure 6(d). The DSM values are displayed in light blue, the produced DTM in red, and the ICC reference DTM in black. The profiles show that the algorithm could properly detect and eliminate the non-ground regions from original data set. Furthermore, the assessment procedure is continued by analyzing the difference between produced DTM and ICC reference data which is computed with $diff = DTM - ICC$. Accordingly some statistical parameters have been calculated form the $diff$ image (cf. Table 1).

min	*-18.00m*
max	*19.00m*
mean	*-0.23m*
median	*-0.09m*
standard deviation	*1.74m*
RMSE	*1.76m*

Table 1: Statistical evaluation of produced DTM

Figure 8 illustrates the histogram of the $diff$ image. It shows that for most of the pixels the differences are around $zero$. This is proved by the average value which is computed as $-0.23m$. The maximum and minimum values belong to the non-ground objects connected to the image boundary. As explained, these objects might not be completely eliminated from the final DTM. In practice, it is recommended to process a bigger area to be sure all the 3D objects in desired area are entirely located inside the scene. the other problem as explained is regarding to the high elevated roads that are eliminated from produced DTM which is not the case in ICC reference DTM (cf. Figuers 6(c) and 6(d)).

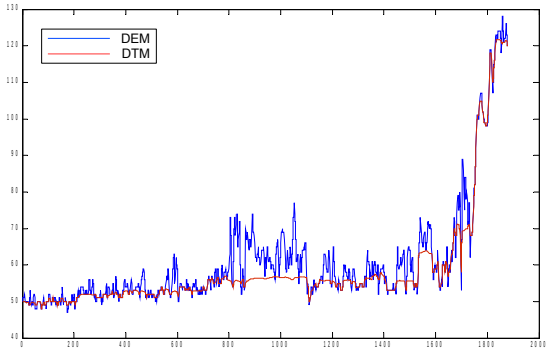

(a) DEM vs. produced DTM

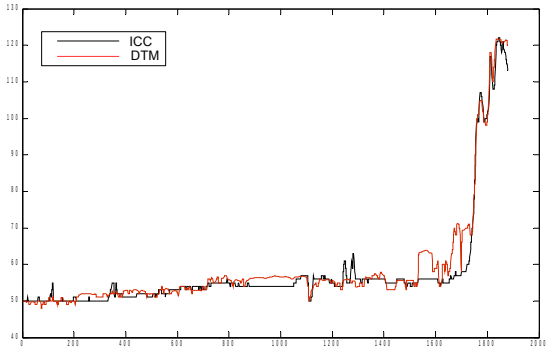

(b) produced DTM vs. ICC reference DTM

Figure 7: A sample profile to compare DSM, produced DTM and ICC reference DTM

5 CONCLUSION

In this paper a novel approach is proposed for automated DTM generation from the DSM produced from CARTOSAT-1 stereo images. The 3D non-ground objects as well as below the ground outliers are eliminated iteratively from the surface model. The filtering process is applied from four corners of the DSM image to be sure that all the non-ground objects are removed.
Our algorithm eliminates almost all obvious non-ground regions, such as buildings and most vegetation areas. Shape and size of the objects are irrelevant in our approach. Large buildings as well as small ones, elongated buildings as well as shortened ones and high buildings as well as low ones are properly eliminated (cf. Figure 6(c)). Only objects connected to the image boundary are not completely eliminated from the final DSM. In practice, it is recommended to process a bigger area to be sure all the 3D objects in desired area are entirely located inside the scene. Ground objects that have similar characteristics as buildings, such as high elevated roads are also eliminated.
The only parameter that is inserted into the process is the threshold value ($thresh$) which is the criterion to differentiate between non-ground and ground regions.
In residential hilly areas where some smoothing filtering has been carried out before DTM generation, the height discontinuities belonging to the 3D objects are blurred as well. In such cases selecting an appropriate threshold value is critical. Therefore, it is recommended to avoid any smoothing filtering that causes losing the sharpness of the edges of the non-ground objects.

References

Arefi, H. and Hahn, M., 2005. A morphological reconstruction algorithm for separating off-terrain points from terrain points in laser scanning data. In: International Archives of Photogrammetry, Remote Sensing and Spatial Information Sciences, Vol. 36 (3/W19).

Arefi, H., Engels, J., Hahn, M. and Mayer, H., 2007. Automatic DTM generation from laser-scanning data in residential hilly area. In: International Archives of Photogrammetry, Remote Sensing and Spatial Information Sciences, Vol. 36 (4/W45).

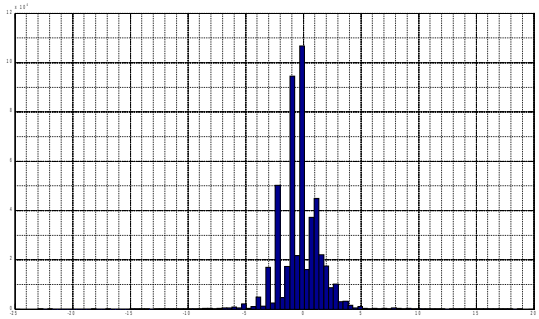

Figure 8: Histogram representing the difference between produced DTM and ICC reference DTM

Axelsson, P., 1999. Processing of laser scanner data - algorithms and applications. ISPRS Journal of Photogrammetry and Remote Sensing 54, pp. 138–147.

Bartels, M. and Wei, H., 2006. Segmentation of LIDAR data using measures of distribution. In: International Archives of Photogrammetry and Remote Sensing and Spatial Information Sciences, Vol. 36 (7), pp. 426 – 431.

d'Angelo, P., Schwind, P., Krauss, T., Frithjof, B. and Reinartz, P., 2009. Automated DSM based Georeferencing of CARTOSAT-1 Stereo Scenes. In: ISPRS Hannover Workshop 2009 – High-Resolution Earth Imaging for Geospatial Information.

Grohman, G., Kroenung, G. and Strebeck, J., 2006. Filling SRTM voids: The delta surface fill model. Photogrammetric Engineering and Remote Sensing 72(3), pp. 213–216.

Kilian, J., Haala, N. and Englich, M., 1996. Capture and evaluation of airborne laser scanner data. In: International Archives of Photogrammetry, Remote Sensing and Spatial Information Sciences, Vol. 31 (B3), pp. 383–388.

Kraus, K. and Pfeifer, N., 1998. Determination of terrain models in wooded areas with airborne laser scanner data. ISPRS Journal of Photogrammetry and Remote Sensing 53, pp. 193–203.

Lantuejoul, C. and Maisonneuve, F., 1984. Geodesic methods in image analysis. Pattern recognition 17, pp. 117–187.

Robinson, K. and Whelan, P. F., 2004. Efficient morphological reconstruction: a downhill filter. Pattern Recognition Letters 25(15), pp. 1759–1767.

Sithole, G., 2001. Filtering of laser altimetry data using a slope adaptive filter. In: International Archives of the Photogrammetry, Remote Sensing and Spatial Information Sciences, Vol. 34 (3-W4), pp. 203–210.

Terrasolid, 2007. Processing laser and images. www.terrasolid.fi. Terrascan software for processing of laser data.

Vincent, L., 1993. Morphological grayscale reconstruction in image analysis: Applications and efficient algorithms. IEEE Transactions on Image Processing 2, pp. 176–201.

Vosselman, G., 2000. Slope based filtering of laser altimetry data. In: International Archives of Photogrammetry, Remote Sensing and Spatial Information Sciences, Vol. 33 (B3), pp. 935–942.

Wack, R. and Wimmer, A., 2002. Digital terrain models from airborne laser scanner data - a grid based approach. In: International Archives of Photogrammetry, Remote Sensing and Spatial Information Sciences, Vol. 34 (B3), pp. 293 – 296.

Zhang, K., Chen, S., Whitman, D., Shyu, M., Yan, J. and Zhang, C., 2003. A progressive morphological filter for removing non-ground measurements from airborne lidar data. IEEE Transaction on Geoscience and Remote Sensing 41(4), pp. 872–882.